Time-Dependent Characteristics of the Nonequilibrium Condensation in Subsonic Flows

Seung-Cheol Baek, Soon-Bum Kwon
Department of Mechanical Engineering, Kyungpook National University,
1370, Sankyuk-dong, Daegu 702-701, Korea
Toshiaki Setoguchi
Department of Mechanical System Engineering, Saga University, 1, Honjo, Saga 840-8502, Japan
Heuy-Dong, Kim*
School of Mechanical Engineering, Andong National University,
Songchun-dong, Andong 760-749, Korea

High-speed moist air or steam flow has long been of important subject in engineering and industrial applications. Of many complicated gas dynamics problems involved in moist air flows, the most challenging task is to understand the nonequilibrium condensation phenomenon when the moist air rapidly expands through a flow device. Many theoretical and experimental studies using supersonic wind tunnels have devoted to the understanding of the nonequilibrium condensation flow physics so far. However, the nonequilibrium condensation can be also generated in the subsonic flows induced by the unsteady expansion waves in shock tube. The major flow physics of the nonequilibrium condensation in this application may be different from those obtained in the supersonic wind tunnels. In the current study, the nonequilibrium condensation phenomenon caused by the unsteady expansion waves in a shock tube is analyzed by using the two-dimensional, unsteady, Navier-Stokes equations, which are fully coupled with a droplet growth equation. The third-order TVD MUSCL scheme is applied to solve the governing equation systems. The computational results are compared with the previous experimental data. The time-dependent behavior of nonequilibrium condensation of moist air in shock tube is investigated in details. The results show that the major characteristics of the nonequilibrium condensation phenomenon in shock tube are very different from those in the supersonic wind tunnels.

Nomenclature

a : Speed of sound
C_p : Specific heat capacity at constant pressure $[J/(kg \cdot K)]$
E_t : Total energy per unit volume $[J/m^3]$
E, F : Numerical flux

---

* Corresponding Author,
E-mail : kimhd@andong.ac.kr
TEL : +82-54-820-5622; **FAX :** +82-54-823-5495
School of Mechanical Engineering, Andong National University, Songchun-dong, Andong 760-749, Korea.

g : Condensate mass fraction [-]
h^* : Tube height [mm]
H : Source term
I : Nucleation rate $[1/(m^3 \cdot s)]$
J : Jacobian
k : Boltzmann constant $[J/K]$
L : Latent heat $[J/kg]$
m : Mass [kg] or molecular weight [kg/kmol]
Pr : Prandtl number
p : Static pressure $[Pa]$
λ : Coefficient of second viscosity
ξ, η : Generalized coordinates [-]

ζ : Condensation coefficient [-]

ρ : Density [kg/m^3]

σ : Surface tension [N/m]

ϕ : Relative humidity [%]

ω : Specific humidity [-]

Sub/superscripts

0 : Stagnation state

∞ : Infinite plane surface

l : Liquid

m : Mixture

r : Droplet radius

v : Vapour

s : Saturation

1. Introduction

Rapid expansion of a condensible gas, like vapour or moist air, is often encountered in such as a supersonic nozzle or a transonic wing and usually causes nonequilibrium condensation of moist air. The nonequilibrium condensation almost always accompanies strong irreversibility as well as some instability in the flow field and quite complicated wave motions result from the heat transfer processes of the latent heat release of the moist air. Up to now, many studies related to the nonequilibrium condensation and instabilities have been carried out using supersonic wind tunnels (Wegener and Mack 1958; Frank 1985; Wegener and Pouring 1964).

Unlike equilibrium condensation, the nonquilibrium condensation does not occur on a saturation line being thermodynamically equilibrium state, but undergoes a spontaneous condensation or a homogeneous condensation process due to coalescence of vapour molecules around a discrete condensation nucleus (Zierep and Lin 1967; Matsuo et al. 1985). This condensation process is made at a finite speed being nearly the same as a general chemical reaction rate and thus has a reaction barrier that is very similar to the activation energy of the reaction. Such a condensation of moist air occurs at a supersaturation or a supercooling state, and thereby this kind of process is called as nonequilibrium condensation.

The flow field of the nonequilibrium condensa-

tion of moist air in a supersonic wind tunnel is schematically shown in Fig. 1. The flow is accelerated to a supersonic speed through the nozzle throat and, the nonequilibrium condensation starts to form downstream of the nozzle throat. In this case, the static pressure along the nozzle axis begins to rise due to the effect of the latent heat release of the nonequilibrium condensation, and reaches a peak value before decreasing downstream, where the flow is again accelerated to a supersonic speed. The degree of local supersaturation S, of the flow has a peak value at the location where the static pressure begins to increase. The nucleation rate I, increases upstream of the location where the nonequilibrium condensation occurs, having a peak value before it rapidly decreases in the region of the rising static pressure. The liquid mass fraction, g, suddenly begins to increase at the location where the static pressure begins to increase.

It is clearly known that the onset of nonequilibrium condensation is the location (see point a)
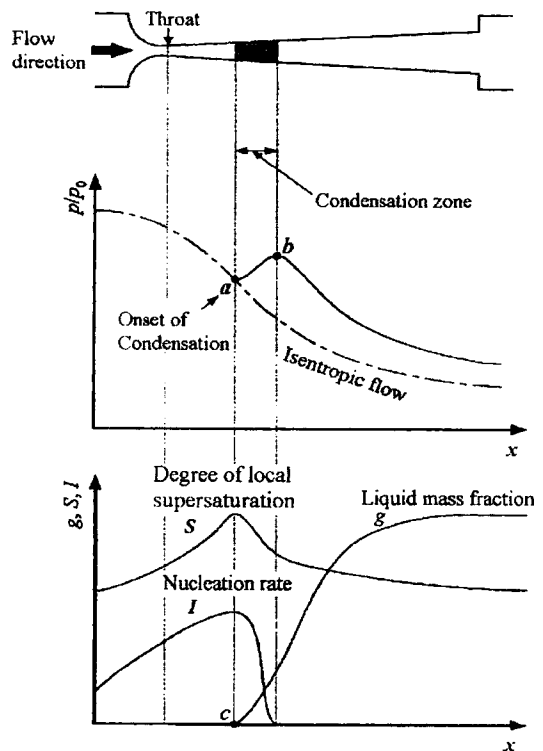

Fig. 1 Condensation in a supersonic nozzle

where the local static pressure begins to rise. This location corresponds to the point that the liquid mass fraction starts to increase (see point c). It is, thus, believed from Fig. 1 that the onset of the nonequilibrium condensation can be characterized by both the local static pressure and liquid mass fraction.

The static pressures have been used to define the onset point of the nonequilibrium condensation so far, because it is the simplest way to measure the onset of the nonequilibrium condensation in supersonic wind tunnels (Hill 1966; Matsuo et al. 1985). The nonequilibrium condensation in the supersonic wind tunnels is a kind of heat addition process, accompanying complex wave motions. Some pressure waves can propagate both upstream and downstream of the region of the nonequilibrium condensation, even at supersonic flow speed. The resulted flow is essentially unsteady.

Unlike the condensible gas flows in the supersonic wind tunnels above, the nonequilibrium condensation can also occur in shock tube flow. In this case, understanding of how the time-dependent static pressures are generated is very important since the details of the nonequilibrium condensation should be interpreted through them. It is undoubtedly desirable to examine the non-equilibrium condensation in a time-dependent frame. Unfortunately, unsteady static pressure data highly lacking and at most, existing data are too sparse, and involving a considerable measurement uncertainty.

Figure 2 shows typical experimental example of the nonequilibrium condensation occurring in the shock tube (Matsuo et al. 1982). In the experiment, the high-pressure tube was filled with atmospheric moist air, and the low-pressure tube was reduced below atmospheric pressure. With diaphragm rupture, the moist air is accelerated by the unsteady expansion waves propagating toward the high-pressure tube, and then the non-equilibrium condensation results from the expansion waves. The static pressure was measured by using a pressure transducer at the location of 140 mm upstream of the diaphragm and a light scattering method (Barschdorff and Fillipov
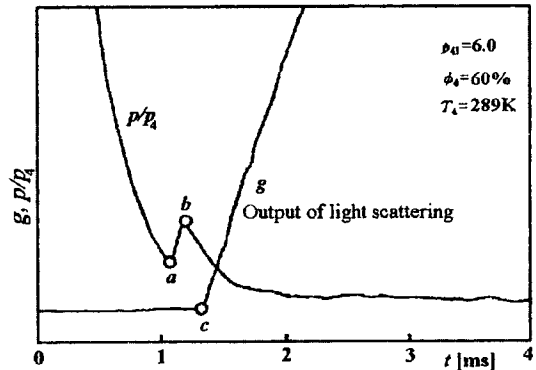

Fig. 2 Time histories of static pressure and liquid mass fraction in shock tube

1970) was to detect the liquid mass fraction of the condensation. Thus, output of the light scattering reflects the liquid mass fraction of the nonequilibrium condensation, which is formed at the high-pressure tube.

There is a considerable discrepancy between the locations of the points a and c, which are the rising static pressure and liquid mass fraction, respectively. When the nonequilibrium condensation occurs, consequently a series of pressure waves generate in the flow field, propagating both upstream and downstream. The pressure waves moving upstream are coalesced at a certain location, because the flow is subsonic speed. This causes local pressure jump and thus the two points (ponts a and c) are not in agreement. It is believed that in shock tube flow the location where the local static pressure begins to rise does not correspond to the point of the rising liquid mass fraction. Therefore, if the onset of the nonequilibrium condensation is explained as the local pressure rise, which has long been accepted in the steady supersonic wind tunnels, an obvious confliction is made in shock tube flow.

There is no detailed information regarding the nonequilibrium condensation in shock tube flow. The major characteristic quantities regarding the nonequilibrium condensation, involving their spatial distributions, and associated pressure losses, has not ever been investigated so far. Further study is necessary to clearly understand the major characteristics of the time-dependent nonequili-

brium condensation caused by the unsteady expansion wave. Recently, Kim et al. (2001) have tried to compute the nonequilibrium condensation flow in Ludwieg Tube and they have used a TVD MUSCL scheme to solve the unsteady two-dimensional Navier-Stokes equations. Their results have predicted the measured ones with a good accuracy.

In the present study, computations are applied to understand the major characteristics of the time-dependent nonequilibrium condensation in a shock tube flow and to investigate the effect of the initial relative humidity on the nonequilibrium condensation and shock Mach number. Two-dimensional compressible Navier-Stokes equations, fully coupled with a droplet growth equation, are solved by a third-order TVD MUSCL scheme, and the computational results are compared with the previous experimental ones. In computation, a second-order central difference scheme is applied to viscous terms, and a second-order fractional time step is employed for time integration.

2. Governing Equations and Numerical Methods

2.1 Governing equations

For simplicity of the present computational analysis, several assumptions are made; there is no velocity slip and no temperature difference between condensate particles and medium gas flows, and thus the energy relaxation processes between two phases are not considered in the present analysis. Due to very small condensate particles, the effect of the particles on pressure field of flow can be neglected. The resulting governing equations are the unsteady, two-dimensional, compressible, Navier-Stokes equations, which are given by Eq. (1) (Setoguchi et al. 2001a ; Setoguchi et al. 2001b):

$$\frac{\partial Q}{\partial t} + \frac{\partial E}{\partial x} + \frac{\partial F}{\partial y} = \frac{1}{\mathrm{Re}}\left(\frac{\partial R}{\partial x} + \frac{\partial S}{\partial y}\right) + H \quad (1)$$

where

$$Q = \begin{bmatrix} \rho_m \\ \rho_m u \\ \rho_m v \\ \rho_m E_t \\ \rho_m g \\ \rho_m D_1 \\ \rho_m D_2 \\ \rho_m D_3 \end{bmatrix}, \; E = \begin{bmatrix} \rho_m u \\ \rho_m u^2 + p \\ \rho_m u v \\ u(E_t + p) \\ \rho_m u g \\ \rho_m u D_1 \\ \rho_m u D_2 \\ \rho_m u D_3 \end{bmatrix}, \; F = \begin{bmatrix} \rho_m v \\ \rho_m u v \\ \rho_m v^2 + p \\ v(E_t + p) \\ \rho_m v g \\ \rho_m v D_1 \\ \rho_m v D_2 \\ \rho_m v D_3 \end{bmatrix} \quad (2)$$

$$H = \begin{bmatrix} 0 \\ 0 \\ 0 \\ 0 \\ \rho_m \dot{g} \\ \rho_m \dot{D}_1 \\ \rho_m \dot{D}_2 \\ \rho_m \dot{D}_3 \end{bmatrix}, \; R = \begin{bmatrix} 0 \\ \tau_{xx} \\ \tau_{xy} \\ \alpha \\ 0 \\ 0 \\ 0 \\ 0 \end{bmatrix}, \; S = \begin{bmatrix} 0 \\ \tau_{yx} \\ \tau_{yy} \\ \beta \\ 0 \\ 0 \\ 0 \\ 0 \end{bmatrix} \quad (3)$$

where

$$\alpha = u\tau_{xx} + v\tau_{yx} + \frac{\mu}{(\gamma - 1)\,\mathrm{Pr}}\frac{\partial T}{\partial x}$$
$$\beta = u\tau_{xy} + v\tau_{yy} + \frac{\mu}{(\gamma - 1)\,\mathrm{Pr}}\frac{\partial T}{\partial y} \quad (4)$$

In Eq. (4), μ and Pr are defined as

$$\mu = \mu_{laminar} + \mu_{turbulent},$$
$$\frac{\mu}{\mathrm{Pr}} = \frac{\mu_{laminar}}{\mathrm{Pr}_{laminar}} + \frac{\mu_{turbulent}}{\mathrm{Pr}_{turbulent}} \quad (5)$$

Further,

$$E_t = \rho_m C_{p0} T - p + \frac{1}{2}\rho_m (u^2 + v^2) - \rho_m g L \quad (6)$$

$$p = G\left[E_t - \frac{1}{2}\rho_m (u^2 + v^2) + \rho_m g L\right] \quad (7)$$

$$G = \left(1 - g\,\frac{m_m}{m_v}\right) \Big/ \left(\frac{1}{\gamma - 1} + g\,\frac{m_m}{m_v}\right) \quad (8)$$

where subscripts v and m refer to vapour phase and mixture, respectively. The latent heat L is given by a function of temperature (Prupppacher and Klett 1980):

$$L(T) = L_0 + L_1 T \; [\mathrm{J/kg}]$$
$$L_0 = 3105913.39 \; [\mathrm{J/kg}] \quad (9)$$
$$L_1 = -2212.97 \; [\mathrm{J/kg}]$$

The condensate mass fraction g is given by a certain rate equation, expressed by Eq. (10) (Adam 1999).

$$\dot{g} = \frac{dg}{dt} = \frac{\rho_l}{\rho_m}\left(\frac{4\pi}{3}r_c^3 I + \rho_m D_1 \frac{dr}{dt}\right) \quad (10)$$

In Eq. (3), D_1, D_2, and D_3 are given as:

$$\dot{D_1} = \frac{dD_1}{dt} = \frac{4\pi r_c^2 I}{\rho_m} + D_2 \frac{dr}{dt} \quad (11)$$

$$\dot{D_2} = \frac{dD_2}{dt} = \frac{8\pi r_c^2 I}{\rho_m} + D_3 \frac{dr}{dt} \quad (12)$$

$$\dot{D_3} = \frac{dD_3}{dt} = \frac{8\pi I}{\rho_m} \quad (13)$$

Nucleation rate I, critical radius of the nuclei r_c and radius growth rate $\dot{r}$ are given as (Adam 1999 ; Sislian 1975 ; Mills and Seban 1967):

$$I = \frac{1}{\rho_l}\left(\frac{2m_v\sigma}{\pi}\right)^{1/2}\left(\frac{p_v}{kT}\right)^2 \exp\left[\frac{-4\pi r_c^2\sigma}{3kT}\right] \quad (14)$$

$$r_c = \frac{2\sigma}{\rho_l\Re_v T \ln(p_l/p_{s,\infty})} \quad (15)$$

$$\dot{r} = \frac{dr}{dt} = \frac{\alpha}{\rho_c}\frac{p_v - p_{s,r}}{(2\pi\Re_v T)^{1/2}} \quad (16)$$

In the above equations, m, $\Re$, k and $p_{s,\infty}$ are the molecular weight, the gas constant, the Boltzmann constant and the flat film equilibrium vapour pressure, respectively. In the present computations, the nucleation coefficient is given as 1.0 (Adam 1999). The density of liquid phase is given as a function of temperature t (Prupppacher and Klett 1980):

$$\rho_l(T) = \frac{A_0 + A_1 t + A_2 t^2 + A_3 t^3 + T_4^4 + A_5 t^5}{1 + B_0 t} \text{ [kg/m}^3\text{]}, \ (t \geq 0\text{°C})$$
$$\rho_l(T) = A_6 + A_7 t + T_8 t^2 \text{ [kg/m}^3\text{]}, \ (t < 0\text{°C}) \quad (17)$$

where t is the temperature given by °C and the coefficients are given by ;

$$A_0 = 999.8396, \ A_1 = 18.224944, \ A_2 = -7.92221\times 10^{-3}$$
$$A_3 = -55.44846\times 10^{-6}, \ A_4 = 149.7562\times 10^{-9},$$
$$A_5 = -393.2952\times 10^{-12}, \ A_6 = 999.84, \ A_7 = 0.086, \quad (18)$$
$$A_8 = -0.0108, \ B_0 = 18.159725\times 10^{-3}$$

The surface tension σ is defined by $\zeta\sigma_\infty$, where σ_∞ is an infinite flat-film surface tension and ζ the coefficient of surface tension (Schnerr and Dohrmann 1990), given by ;

$$\sigma_\infty(T) = \{76.1 + 0.155(273.15 - T)\}\times 10^{-3},$$
for $T \geq 249.39K$
$$\sigma_\infty(T) = \{(1.1313 - 3.7091\times 10^{-3}\times T) \quad (19)$$
$$\times T^4\times 10^{-4} - 5.6464\}\times 10^{-6},$$
for $T < 249.39K$

In Eq. (14), $p_{s,\infty}$ is also given as (Prupppacher and Klett 1980);

$$P_{s,\infty}(T) = \exp\left(A_9 + A_{10}T + A_{11}T^2 + B_1\ln(T) + \frac{C_0}{T}\right)$$
$$\text{[N/m}^3\text{]} \quad (20)$$
$$A_9 = 21.125, \ A_{10} = -2.7246\times 10^{-2}, \ A_{11} = 1.6853\times 10^{-5}$$
$$B_1 = 2.4576, \ C_0 = -6094.4642$$

where T is the temperature given by Kelvin. Using the flat film equilibrium vapour pressure $p_{s,\infty}$ above, the saturation vapour pressure of condensate droplet with a radius of r is given by Thompson-Gibbs equation (Rusak and Lee 2000);

$$p_{s,r} = p_{s,\infty}\exp\left(\frac{2\sigma_\infty}{\rho_l\Re_v T_r}\right) \quad (21)$$

In computations, the value of ζ is given as 1.0 in the present analysis.

The governing equation systems above are mapped from the physical plane (x, y) into a computational plane (ξ, η) of a general transform.

$$\frac{\partial\hat{Q}}{\partial t} + \frac{\partial\hat{E}}{\partial\xi} + \frac{\partial\hat{F}}{\partial\eta} = \frac{1}{Re_o}\left(\frac{\partial\hat{R}}{\partial\xi} + \frac{\partial\hat{S}}{\partial\eta}\right) + \hat{H} \quad (22)$$

$$\hat{Q} = JQ, \ \hat{E} = J(\xi_x E + \xi_y F)$$
$$\hat{F} = J(\eta_x E + \eta_y F)$$
$$\hat{R} = J(\xi_x R + \xi_y S), \ \hat{S} = J(\eta_x R + \eta_y S) \quad (23)$$
$$J^{-1} = |x_\xi y_\eta - y_\xi x_\eta|$$

To close the governing equations above, Baldwin-Lomax model is employed in computations (Baldwin and Lomax 1978). A third-order TVD (total variation diminishing) finite difference scheme with MUSCL (Setoguchi et al. 2001a ; Yee 1989) is used to discrete the spatial derivatives, and a second order-central difference scheme for the viscous terms. A second-order upwind TVD scheme is applied to the droplet growth equation (Setoguchi et al. 2001a ; Setoguchi et al. 2001b), and a second order fractional step is employed for time integration.

2.2 Numerical method and computational conditions

Figure 3 shows the computational grid of the present shock tube flow. In computation, the number of grids employed are 1001×61, highly clustered near the wall. This was obtained from several kinds of preliminary computational tests for the grid-independent solutions. The shock tube consists of two-dimensional duct of 38 mm high ($=h^*$) and 1000 mm long, and the high-pressure tube is of 700 mm in length. These dimensions are based on the previous experiment by Matsuo et al. (1982) The diaphragm locates between the high and low pressure tubes, and its location is an origin ($x=0$) for the present computational analysis.

The pressures in the high and low-pressure tubes are defined as p_4 and p_1, respectively. The pressure ratio $p_{41}(=p_4/p_1)$ is kept constant at 6.0, where p_4 is kept constant at atmospheric pressure ($=101.3$ kPa) and, the temperature in the high-pressure tube T_4 is varied between 288.34 and 297.8 K. The initial relative humidity of moist air ϕ_4 is varied between 20 and 80%. The specific humidity of moist air ω_4 is defined as mass of vapour component per unit mass of the moist air involved, at the initial condition of the high-pressure tube. Thus the obtained specific humidity is in the range of $2.73 \times 10^{-3} < \omega_4 < 11.1 \times 10^{-3}$.

The height h^* of the duct is yielded as a characteristic length scale in the present analysis. Moist air is used as a working fluid and assumed to be thermally and calorically perfect. Inlet and outlet boundaries are constrained to the free boundary conditions. No-slip wall velocity is assumed on adiabatic wall condition of no heat transfer. Further, condensate mass fraction $g=0$ is given at the solid walls and the symmetry condition on the shock tube centerline.
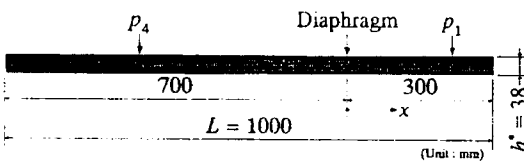

Fig. 3   The computational shock tube

3. Results and Discussion

Figure 4 shows the predicted wave diagram of the present shock tube flow for the purpose of comparison with the experimental results obtained by Matsuo et al. (1982) Both the computational and experimental results represent the loci of the points a and c, respectively, which were indicated in Fig. 2. The locus of the point a refers to the location where the static pressure begins to rise due to nonequilibrium condensation in the high-pressure tube, and the locus of the point c is the location of the rising liquid mass fraction. From both the predicted and measured wave diagrams, it is found that the present computation qualitatively predicts the experimental results, and the agreement between both the results seems to be not good. This results from the fact that zero-time for the diaphragm rupture is assumed in computations, while in experiments it takes a finite time to rupture the diaphragm. This fact is also found from the locus of the experimental results of the points a and c. Both the results show that the region between the two loci of the points a and c become broader, as the expansion waves move upstream. This is due to broadening of the unsteady expansion fan caused by the diaphragm rupture.

The predicted and measured time histories of the static pressures at the location of $x = -140$ mm upstream of the diaphragm are compared in
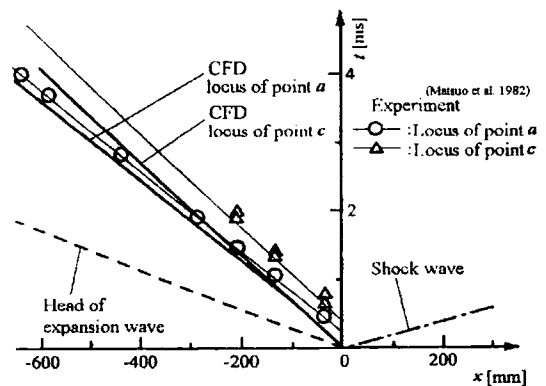

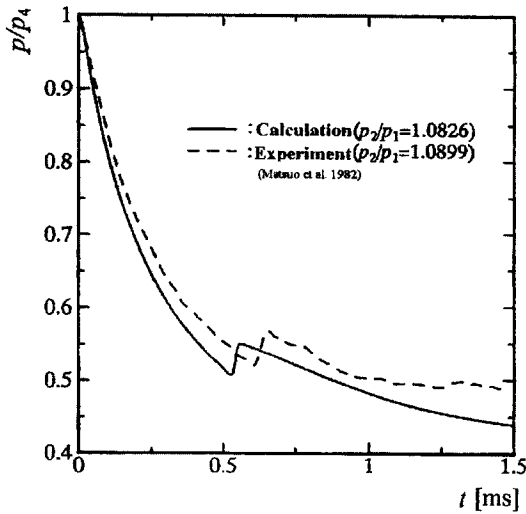Fig. 4   The comparison between predicted and measured pressure histories

Fig. 5 Time history of predicted and measured static pressure at $x=-140$ mm

Fig. 5, in which the local pressure is normalized by the initial pressure p_4 in the high-pressure tube, and the time t starts after the head of the expansion wave reach at the location of $x=-140$ mm. Note that p_2 is defined as the pressure just behind the shock wave propagating toward the low pressure tube, and p_1 is the initial pressure in the low pressure tube. It should be further noted that the predicted and measured pressure ratios of p_2/p_1 are 1.0826 and 1.0899, respectively. The present computation qualitatively predicts the measured pressure history, but the agreement is not good. In considering the present complicated flow field of the nonequilibrium condensation and the diaphragm rupture time as well, it is believed that the present computation predicts the complicated nonequilibrium condensation flow with an acceptable accuracy.

Figures 6, 7 and 8 present the predicted spatial and temporal dependence of the nonequilibrium condensation for different initial relative humidity, in which the normalized static pressure p/p_4, degree of local supersaturation S, condensate mass fraction g and nucleation rate I are plotted with time t and distance x/h^*. The condensate mass fraction g is normalized by using a certain maximum value g_{max}, the dashed lines indicate the predicted result for dry-airflow, and the direction
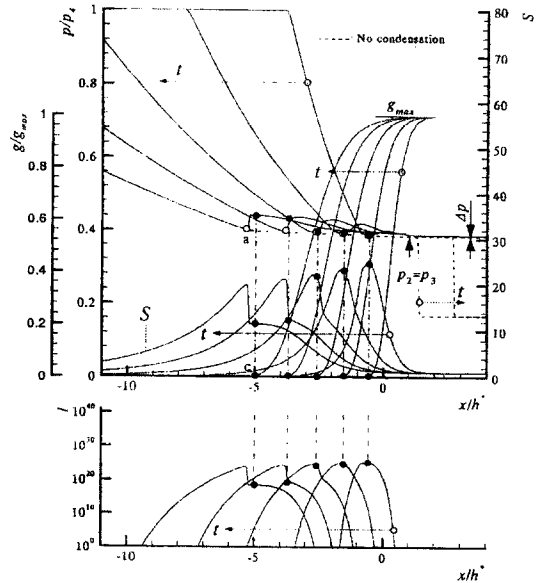

Fig. 6 Temporal and spatial characteristics of nonequilibrium condensation ($\phi_4=20\%$, $T_4=293$ K, $\omega_4=2.73\times10^{-3}$)
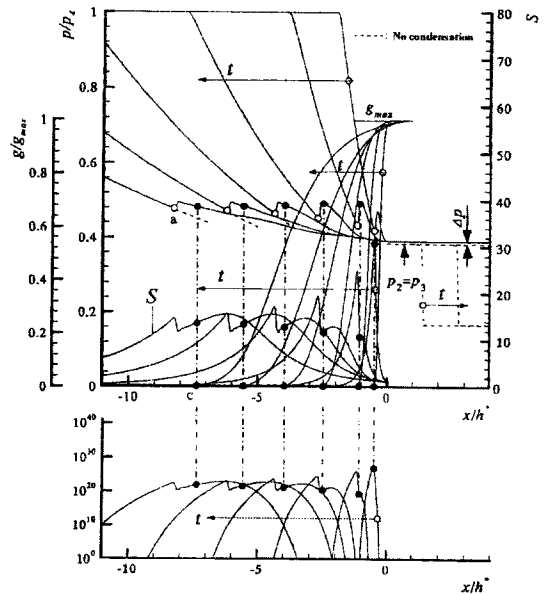

Fig. 7 Temporal and spatial characteristics of nonequilibrium condensation ($\phi_4=40\%$, $T_4=293$ K, $\omega_4=5.47\times10^{-3}$)

of the arrow indicates an increase in time. The pressure p_2 and p_3 are defined just behind the shock wave and the contact surface in the low-pressure tube, respectively, and Δp means the
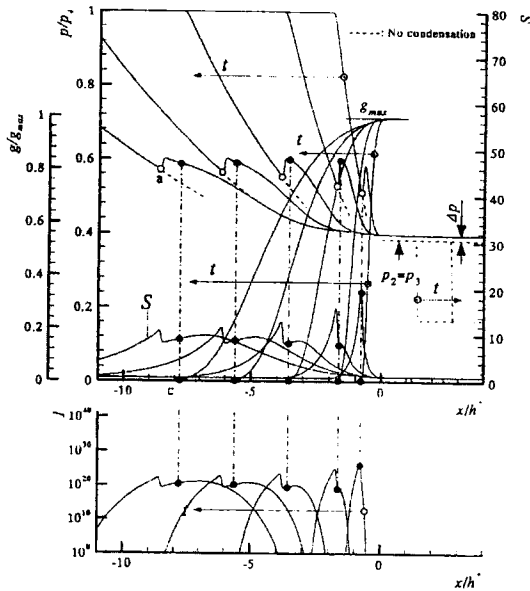
Fig. 8 Temporal and spatial characteristics of non-equilibrium condensation (ϕ_4=80%, T_4=293 K, ω_4=10.98×10⁻³)

pressure difference, just behind the shock wave, for both cases of moist air and dry airflows.

For ϕ_4=20%, T_4=293 K and ω_4=2.73×10⁻³, presented in Fig. 6, the static pressure rapidly decreases due to the unsteady expansion waves propagating toward the high-pressure tube, and has a local minimum value (see the blank circle). Then it increases to a certain peak value, before decreasing again. Both the points of the local minimum and peak pressures move upstream with an increase in time. It seems that the gradient in the pressure drop decreases with an increase in time. It is interesting to note that the local peak pressure due to the nonequilibrium condensation somewhat increases with time.

The point that the condensate mass fraction begins to increase is indicated by filled circles (●) and it moves upstream with time. It is worthwhile noting that for each time plotted, the location of the filled circles does not correspond to that of the blank circles (○) and it locates further downstream. This means that the static pressure starts to increase before the condensate mass fraction increases. It is believed that the pressure waves due to the latent heat release of the non-

equilibrium condensation propagate upstream and contribute to the time-mean static pressure rise upstream of the location where the condensate mass fraction increases. Meanwhile, the spatial distribution of the degree of local supersaturation S shows a peak value near the location where the condensate mass fraction starts to increase, moving upstream with time, but its peak value decreases with time.

It is found that the peak value of the degree of local supersaturation is the same to the location that the condensate mass fraction g starts to increase in the region of $x/h^* > -3.0$. However, in the region of $x/h^* < -3.0$ it locates upstream of the location that the condensate mass fraction g starts to increase. This is due to the generation of the weak discontinuity caused by the non-equilibrium condensation. Similar trend can be also found from the distribution of the condensation nucleation rate I. The location of the maximum nucleation rate does not correspond to the location that the condensate mass fraction starts to increase.

The present computational results significantly differ from those of the previous supersonic wind tunnels. The nonequilibrium condensation occurring in shock tube results from the unsteady expansion waves, in which the flow speed is subsonic. In this case, the latent heat release of the moist air and associated flow field is different from those in supersonic flow.

Figure 7 shows the spatial and temporal distributions of the nonequilibrium condensation for ϕ_4=40%, T_4=293 K and ω_4=5.47×10⁻³. If compared with the results of Fig. 6, somewhat different trend is found in the static pressure jump due to the nonequilibrium condensation. The static pressure jump moves upstream with time, but its magnitude becomes lower with time. The point c that the condensate mass fraction g begins to increase does not correspond to the location of the rising static pressure. It is reasonable to conclude that the onset of the non-equilibrium condensation in a shock tube flow is not the location that the static pressure starts to increase, but the condensate mass fraction g begins to increase.
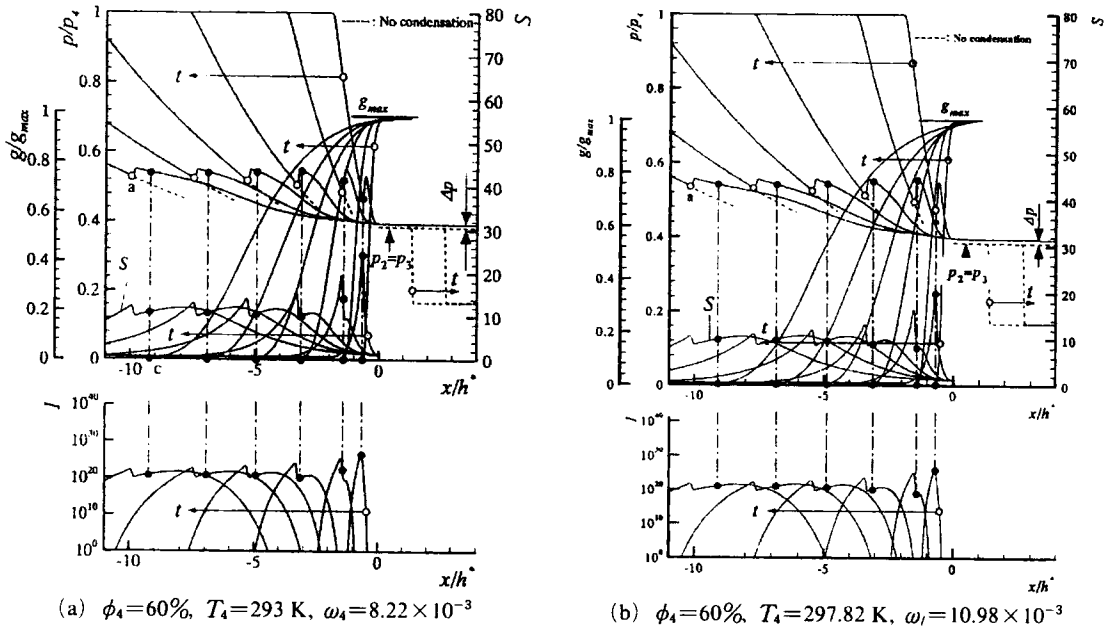
(a) $\phi_4=60\%$, $T_4=293$ K, $\omega_4=8.22\times10^{-3}$ (b) $\phi_4=60\%$, $T_4=297.82$ K, $\omega_l=10.98\times10^{-3}$

Fig. 9 The effect of specific humidity on temporal and spatial characteristics of nonequilibrium condensation

For $\phi_4=80\%$, $T_4=293$ K and $\omega_4=10.98\times10^{-3}$, Fig. 8 shows that with a higher initial relative humidity of the moist air, the static pressure jump becomes higher, the spatial distributions of the degree of local supersaturation and condensation nucleation rate become narrower, compared with the cases of a relatively lower initial humidity. The difference between the moist air and dry air flows is more significant.

The effect of the initial specific humidity on the temporal and spatial characteristics of the nonequilibrium condensation with the same initial relative humidity of $\phi_4=60\%$ are shown in Fig. 9. It is found that the local pressure jump for higher specific humidity, $\omega_4=10.98\times10^{-3}$ is located further upstream with time than for lower one, $\omega_4=8.22\times10^{-3}$. Furthermore, the discrepancies between the location of local highest pressure and the point that the condensate mass fraction starts to increase are more appreciable for higher specific humidity. It can be shown that the pressure difference Δp also increases for higher specific humidity. In the comparison Fig. 8 for $\phi_4=80\%$, $T_4=293$ K, $\omega_4=10.98\times10^{-3}$, with Fig. 9(b) for $\phi_4=60\%$, $T_4=293$ K, $\omega_4=10.98\times10^{-3}$, which are for the same initial specific humidity

and different relative one, it is found that the discrepancies between the highest local pressure and the point that the condensate mass fraction starts to increase become pronounced compared with the those of relatively lower one. However the flow with relatively higher specific humidity induces much higher pressure jump than the one with lower. This is explained that even at the same relative humidity, flow for higher specific humidity contains relatively more moisture, therefore larger amount of heat releases by the nonequilibrium condensation.

Figure 10 represents the time history of flow properties with and without condensation at two upstream locations, $x=-100$ mm and $x=-200$ mm. The initial conditions in high-pressure tube for the case of condensation are $\phi_4=60\%$, $T_4=293$ K and $\omega_4=8.22\times10^{-3}$, respectively. The static pressure without condensation decreases monotonously with time due to the upstream propagation of the unsteady expansion waves in the high-pressure tube, while the local pressure jump occurs with condensation. It is also found that the amounts of pressure jump and entropy increase at $x=-200$ mm are much lower than that at $x=-100$ mm. This is due to the reduction of heat
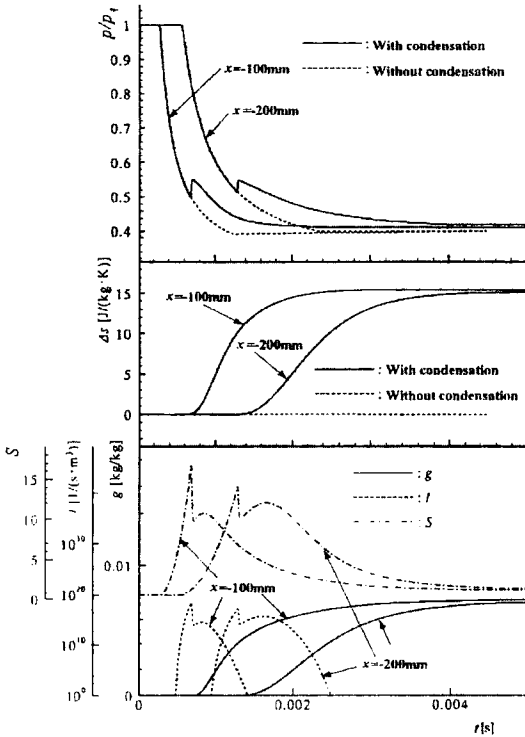
Fig. 10 Time history of flow properties with and without condensation at two upstream locations

Fig. 11 The effect of the initial relative humidity on the adiabatic shock Mach number M_s

release by attenuation of the expansion waves during the upstream propagation. It can also be seen that the maximum local degree of supersaturation and condensate mass fraction at $x = -100$ mm much higher than those at $x = -200$ mm.

Figure 11 shows the effect of the initial relative humidity on the adiabatic shock wave, which propagates toward the low-pressure tube. The shock Mach number M_s is given as a function of the initial relative humidity of moist air. The dashed line means the result of theoretical prediction using one-dimensional gas dynamics theory. For a comparatively low initial humidity of moist air, the shock Mach numbers are nearly the same as to the theoretical prediction, but with an increase in the relative humidity, the shock Mach number seems to be a function of the initial relative humidity in the high-pressure tube. For instance, in cases of the initial relative humidity of $\phi_4 = 60$ to 80%, the shock Mach number increases 20% to 30%, compared with the dry
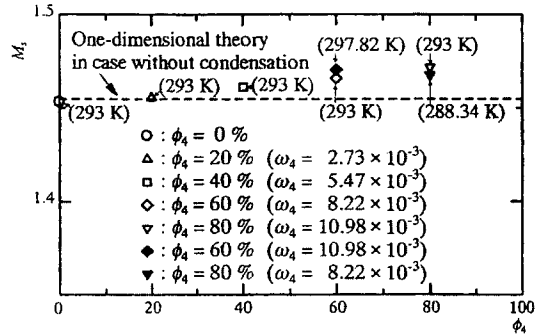
air flow. Since the higher the initial relative humidity is, the larger is the latent heat release of nonequilibrium condensation, the resulted pressure waves become stronger, causing the shock wave Mach number to be higher. Therefore it is known that the gas dynamics theory of dry air can't predict the shock Mach number M_s for moist air flow.

For a given initial relative humidity of moist air, the shock Mach number is also affected by the initial specific humidity and temperature in the high-pressure tube. For the same initial relative humidity of $\phi_4 = 60\%$, if the temperature of moist air decreases from 297.8 K to 293 K, the resulted initial specific humidity decreases from 10.98×10^{-3} to 8.22×10^{-3}, the shock Mach number M_s becomes lower by about 10%.

4. Concluding Remarks

The computational analysis is performed to investigate the time-dependent characteristics of nonequilibrium condensation in a shock tube. Two-dimensional, unsteady, compressible, Navier-Stokes equations are fully coupled with a droplet growth equation. The governing equations are solved numerically by the third-order MUSCL type TVD finite difference scheme, with the second-order time fractional time step. The computational results are compared with the previous experimental data.

It is found that the static pressure rise due to nonequilibrium condensation increases with the

initial relative humidity in the high-pressure tube, and it is also affected by the initial specific humidity. For nonequilibrium condensation in shock tube, the location that the static pressure begins to increase does not correspond to the location that the condensate mass fraction starts to increase. It is recommended that the onset of the nonequilibrium condensation should be defined as the location that the condensate mass fraction starts to increase. In the case of a diabatic flow of nonequilibrium condensation in subsonic speed or the flow induced by the unsteady expansion waves, the shock Mach number increases with the initial relative and specific humidities of moist air. The pressure waves generated by the latent heat release of moist air are responsible for this.

References

Adam, S., 1999, "Fukaltat fur Mechanical Engineering," Disseration Universitat Karlsruhe.

Baldwin, B. S. and Lomax, H., 1978, "Thin Layer Approximation and Algebraic Model for Separated Turbulent Flows," *AIAA*, pp. 78~257.

Barschdorff, D. and Fillipov, G. A., 1970, "Analysis of Certain Special Operating Modes of Laval Nozzles with Local Heat Supply," *Journal of Heat Transfer*, Vol. 2, pp. 76~87.

Frank, W., 1985, "Condensation Phenomena in Supersonic Nozzles," *Acata Mechanica*, Vol. 54, pp. 135~156.

Hill P. G., 1966, "Condensation of Water Vapour during Supersonic Expansion in Nozzles," *Jour. of Fluid Mechanics*, Vol. 25, pp. 593~620.

Kim, H. D., Setoguchi, T., Matsuo, S., Baek, S. C. and Kwon, S. B., 2001, "A CFD Study of the Self-Excited Nozzle Flows with Nonequilibrium Condensation," *Proceedings of Int. Conference of Fluid Dynamics and Propulsion*, Cairo, Egypt.

Matsuo, K., Kawagoe, S., Sonoda, K. and Sakao, K., 1985, "Studies of Condensation Shock Waves (part 1, mechanism of their formation)," *Bulletin of JSME*, Vol. 28, pp. 1416~1422.

Matsuo, K., Ikui, T., Setoguchi, T. and Kawagoe, S., 1982, "Relation Between Condensation and Thermal Choking in an Unsteady Subsonic Flow," *Bulletin of JSME*, Vol. 25, No. 203, pp. 744~751.

Mills, A. F. and Seban, R. A., 1967, "The Condensation Coefficient of Water," *Intl. Jour. Heat and Mass Transfer*, Vol. 10, pp. 1815~1827.

Prupppacher, H. and Klet, J. D, 1980, "Microphysics of Clouds and Precipitation," D. Reidel.

Rusak, Z. and Lee, J. C., 2000, "Transonic Flow of Moist Air around a Thin Airfoil with Nonequilibrium and Homogeneous Condensation," *Journal of Fluid Mechanics*, Vol. 403, pp. 173~199.

Setoguchi, T., Matsuo, S. and Kim, H. D., 2001a, "Passive Control of Condensation Shock Wave Oscillations in a Transonic Nozzle," *Journal of Sound and Vibration* (to be published).

Setoguchi, T., Kim. H. D. and Matsuo, S., 2001b, "Passive Control of the Condensation Shock Wave in a Transonic Nozzle," *Applied Scientific Research, International Journal of the Applications of Fluid Dynamics* (to be published).

Sislian, J. P., 1975, "Condensation of Water Vapour With or Without a Carrier Gas in a Shock Tube," *UTIAS Report* 201.

Schnerr, G. H. and Dohrmann, U., 1990, "Transonic Flow around Airfoils with Relaxation and Energy Supply by Homogeneous Condensation," *AIAA Journal*, Vol. 32, pp. 101~107.

Wegener, P. P. and Pouring, A. A., 1964, "Experiments on Condensation of Water Vapour by Homogeneous Nucleation in Nozzles," *Phys. Fluid*, Vol. 8, No. 10, p. 1802.

Wegener, P. P. and Mack, L. M., 1958, "Condensation in Supersonic Hypersonic Wind Tunnels," *Adv. in Applied Mechanics*, Vol. 5, pp. 307~447.

Yee, H. C., 1989, "A Class of High-Resolution Explicit and Implicit Shock-Capturing Methods," *NASA TM-89464*.

Zierep, J, and Lin, S., 1967, "Bestimung des Kondensationsbeginns Kondensation bei Entspannung Feuchter luft in Ueberschallduesen," *Forsch. Ing.-Wes*, Vol. 33, pp. 169~172.